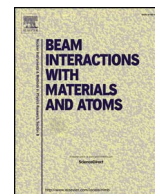




Contents lists available at ScienceDirect

## Nuclear Inst. and Methods in Physics Research B

journal homepage: [www.elsevier.com/locate/nimb](http://www.elsevier.com/locate/nimb)

## Theoretical detection limit of PIXE analysis using 20 MeV proton beams

Keizo Ishii, Keitaro Hitomi\*

Department of Quantum Science and Energy Engineering, Tohoku University, 6-6 Aza-Aoba, Aramaki, Aoba-ku, Sendai 980-8579, Japan

## ARTICLE INFO

## Keywords:

High energy PIXE  
20 MeV proton PIXE  
Detection limit

## ABSTRACT

Particle-induced X-ray emission (PIXE) analysis is usually performed using proton beams with energies in the range 2–3 MeV because at these energies, the detection limit is low. The detection limit of PIXE analysis depends on the X-ray production cross-section, the continuous background of the PIXE spectrum and the experimental parameters such as the beam currents and the solid angle and detector efficiency of X-ray detector. Though the continuous background increases as the projectile energy increases, the cross-section of the X-ray increases as well. Therefore, the detection limit of high energy proton PIXE is not expected to increase significantly. We calculated the cross sections of continuous X-rays produced in several bremsstrahlung processes and estimated the detection limit of a 20 MeV proton PIXE analysis by modelling the Compton tail of the  $\gamma$ -rays produced in the nuclear reactions, and the escape effect on the secondary electron bremsstrahlung. We found that the Compton tail does not affect the detection limit when a thin X-ray detector is used, but the secondary electron bremsstrahlung escape effect does have an impact. We also confirmed that the detection limit of the PIXE analysis, when used with 4  $\mu$ m polyethylene backing film and an integrated beam current of 1  $\mu$ C, is 0.4–2.0 ppm for proton energies in the range 10–30 MeV and elements with  $Z = 16$ –90. This result demonstrates the usefulness of several 10 MeV cyclotrons for performing PIXE analysis. Cyclotrons with these properties are currently installed in positron emission tomography (PET) centers.

## 1. Introduction

A proton beam with energies in the range 2–3 MeV is typically used in particle-induced X-ray emission (PIXE) analysis because the ratio of the characteristic X-ray production cross-section to the continuous X-ray production cross-section is large in this energy regime [1]. However, the characteristic X-ray cross-section decreases rapidly as the proton energy decreases, particularly at energies less than 3 MeV. In this case, the energy loss at the target cannot be neglected in comparison to the incident energy. Therefore, at low energies, a very thin target is required for accurate quantitative analysis. In consideration of the benefit of the low stopping power of protons with energies up to 100 MeV, A. Denker et al. suggested using high energy PIXE analysis for analyzing art works and archaeological objects [2]. This idea enables us to use tens of MeV proton accelerators in PIXE analysis applications. The energies of the protons occurring in cyclotron accelerators in positron emission tomography (PET) centers are fixed in the range 10–20 MeV. These protons are used to produce positron emitting short life radioisotopes. We consider the application of 20 MeV cyclotron proton beams to PIXE analysis. As a consequence of our work, we expect the development of PIXE research at PET centers, of which there are 151 in Japan. The energy loss through Japanese paper of thickness

0.1 mm at this proton energy is 0.13 MeV and the X-ray self-absorption in the sample is about 0.7% in the case of Fe K-X-ray. Hence, accurate quantitative analysis of ancient documents and other samples can be performed. The main components of the continuous background in the X-ray energy spectrum of high energy PIXE analysis are the quasi-free electron bremsstrahlung [3] appearing in the region 0–10 keV and the secondary electron bremsstrahlung [3] in the region of 0–40 keV. The maximum energies of these continuous backgrounds increase as the projectile energy increases. However, the characteristic X-ray production cross-sections become too large in this projectile energy region. Therefore, the detection limit of such high energy proton PIXE analysis is not expected to be significantly worse than that of low energy proton PIXE analysis.

Here, we analytically estimate the detection limit of PIXE analysis with 20 MeV proton beams.

## 2. Detection limit of PIXE

According to standard statistical methods, the peak of a characteristic X-ray can be located on an X-ray energy spectrum using the fact that it is the region where the signal counts are larger than 3 times the root square of the signal counts added to the background counts, within

\* Corresponding author.

E-mail address: [keizo.ishii@qse.tohoku.ac.jp](mailto:keizo.ishii@qse.tohoku.ac.jp) (K. Hitomi).<https://doi.org/10.1016/j.nimb.2017.10.008>Received 31 March 2017; Received in revised form 16 September 2017; Accepted 10 October 2017  
0168-583X/© 2017 Elsevier B.V. All rights reserved.

the width of the detector resolution, or the full-width half maximum (FWHM). Since the signal counts are much smaller than the background counts in the regime of detection limit, we can estimate the detection limits of each component of the PIXE analysis using the following formula [1]:

$$\frac{n_Z}{n_M} = \frac{3}{\sqrt{Q/e \cdot d\Omega \cdot n_M \cdot \delta x \cdot d\sigma_X(Z)/d\Omega \cdot \varepsilon_f(Z) \cdot ab(Z)}} \times \sqrt{\frac{\Delta E_D \cdot d\sigma_B(Z)/(d(\hbar\omega) \cdot d\Omega)}{d\sigma_X(Z)/d\Omega}} \quad (1)$$

where,  $n_Z$  is the concentration of elements with atomic number  $Z$ ,  $n_M$  is the concentration of main atoms in a target,  $Q$  is the integrated beam current,  $e$  is the elementary charge,  $d\Omega$  is the solid angle of the X-ray detector,  $\delta x$  is the target thickness,  $d\sigma_X(Z)/d\Omega$  is the differential cross-section of the characteristic X-ray production for the element with atomic number  $Z$ ,  $\varepsilon_f(Z)$  is the detection efficiency of a characteristic X-ray of an atom with atomic number  $Z$ ,  $ab(Z)$  is the absorption correction produced by materials between the detector and the target, such as a detector window and a chamber window,  $d\sigma_B(Z)/d\Omega d(\hbar\omega)$  is the continuous background yield under the peak of the characteristic X-ray of element  $Z$ , and  $\Delta E_D$  is the detector resolution.

### 3. Characteristic X-ray production cross-sections

In Eq. (1), the differential cross-section of the K X-ray production,  $d\sigma_X(Z)/d\Omega$ , is the product of the fluorescence yield and the inner shell ionization cross-section for element  $Z$ . In the case of L X-ray production cross sections, the coefficients of Coster-Kronig transition between subshells are taken into account. The inner shell ionization cross-section can be calculated accurately using the plane-wave Born approximation, taking into account the binding energy effect, the Coulomb deflection effect, the relativistic effect and the polarization effect. To calculate the detection limit, we use the table of K-shell and L-shell ionization cross-sections produced by D. D. Cohen and M. Harrigan [4] for all elements for proton energies in the range 0.1 ~ 10 MeV. In the case of high energy proton bombardment, the effects of the binding energy and the Coulomb deflection on the inner shell ionization cross-section are very small. We estimate the inner shell ionization cross-sections for proton energies above 10 MeV by normalizing the cross-sections of the Al-K shell obtained in the previous our work[5] to that published by D. D. Cohen and M. Harrigan, in accordance with the scaling law of inner shell ionization cross-sections [6]. According to the scaling law of BEA theory [7], the inner shell ionization cross-sections are maximized when  $\sigma_{\max}^i \approx 4n \times 10^{-20} \text{ cm}^2 \cdot (\text{keV})^2 z_p^2 / U^2$  at  $E/\lambda U = 1$ , where  $n$  is the number of inner shell electrons,  $U$  is the binding energy of the inner shell,  $E$  is the projectile energy,  $z_p$  is the atomic number of the projectile and  $\lambda$  is the ratio of the proton mass to the electron mass. In the case of a 20 MeV proton,  $U(=20 \text{ MeV}/\lambda = 10.89 \text{ keV})$  corresponds to the K-shell ionization potential of germanium and the L<sub>3</sub>-shell ionization potential of osmium, and the production cross-sections of K $\alpha$ - and L $\alpha$ -X-rays are estimated with an uncertainty around 20% for the elements with  $11 < Z < 32$  and  $50 < Z < 76$ . This constant behavior for elements with different atomic numbers makes the system suitable for quantitative analysis.

### 4. Continuous background produced in 20 MeV proton PIXE

Continuous backgrounds in the PIXE spectrum are caused by nuclear bremsstrahlung, atomic bremsstrahlung, secondary electron bremsstrahlung, quasi-free electron bremsstrahlung and the Compton tails of the  $\gamma$ -rays.

The formulae for calculating these bremsstrahlung are as follows. The nuclear bremsstrahlung is calculated using:

$$\frac{d\sigma^{NB}}{d\Omega d(\hbar\omega)} = \frac{a_0^2}{\pi \hbar\omega} \left(\frac{e^2}{\hbar c}\right)^5 \left(1 - \frac{z_T m_p}{z_p m_T}\right)^2 z_p^4 Z_T^2 \left(\frac{m_e c}{m_p v_p}\right)^2 \left\{ (1 + \cos^2 \theta) \ln \left( \frac{2Z_T e^2 m_p v_p}{z_p \hbar^2 \omega} \right) + \left( \frac{3}{2} \sin^2 \theta - 1 \right) \right\} \quad (2)$$

where  $v_p$  is the velocity of the projectile,  $m_p$  is the mass of the projectile,  $Z_T$  is the atomic number of target atom,  $m_T$  is the mass of the target atom,  $\theta$  is the emission angle of photon.

The atomic bremsstrahlung is calculated using:

$$\frac{d\sigma^{AB}}{d\Omega d(\hbar\omega)} = \frac{8a_0^2 \alpha^2}{\pi \hbar\omega} \left(\frac{c}{v_p}\right)^2 \int_{\frac{\omega}{v_p}}^{\infty} \frac{dq}{q} \left\{ 1 - \left(\frac{\omega}{qv_p}\right)^2 + \left(\frac{3}{2}\left(\frac{\omega}{qv_p}\right)^2 - \frac{1}{2}\right) \sin^2 \theta \right\} |S_1(Z_T, q) - S_2(Z_T, q)|^2 \quad (3)$$

where  $q$  is the transfer momentum from the projectile to the atom,  $S_1$  and  $S_2$  are the S-matrix without resonant transitions and with, respectively. The expressions for  $S_1(Z_T, q)$  and  $S_2(Z_T, q)$  are stated in [8].

The secondary electron bremsstrahlung is calculated using:

$$\frac{d\sigma^{SEB}}{d\Omega d(\hbar\omega)}(E_p, \hbar\omega, \theta) = \frac{1}{2\pi} z_p^2 \left(\frac{e^2}{\hbar c}\right)^5 a_0^2 Z_T \frac{m_e c^2}{(\hbar\omega)^2} (C_1 + C_2 \sin^2 \theta) \quad (4)$$

where the expressions for  $C_1$  and  $C_2$  are constant and are stated in [1].

The quasi-free electron bremsstrahlung is given by:

$$\begin{aligned} \frac{d\sigma^{QFEB}}{d\Omega d(\hbar\omega)} &= \frac{1-\beta^2}{1-\beta \cos \theta} \sum_i N_i \int_{-\infty}^{+\infty} dv_x \int_{-\infty}^{+\infty} dv_y \int_{-\infty}^{v_i^{\max}} dv_z \rho_i(v_x, v_y, v_z) \\ &\quad \frac{\hbar\omega'}{\hbar\omega' + U_i + m_e v_z^2} \sigma^{brems}(T_r', \hbar\omega', \theta') \hbar\omega' = \frac{1-\beta \cos \theta}{(1-\beta^2)^{1/2}} \hbar\omega, \quad \cos \theta' \\ &= -\frac{\cos \theta - \beta}{1-\beta \cos \theta} v_i^{\max} = \frac{1}{2} v_p (1 - (\hbar\omega + U_i)/T_r), \quad T_r = \frac{1}{2} m_e v_p^2 T_r' \\ &= T_r (1 - v_z/v_p)^2 \end{aligned} \quad (5)$$

where  $v_x$ ,  $v_y$  and  $v_z$  are the velocity components of inner shell electrons,  $\beta$  is  $v_p/c$  and the expression for  $\sigma^{brems}(T_r', \hbar\omega', \theta')$  is stated in [1].

Fig. 1 shows all the contributions to bremsstrahlung above mentioned in the case of a carbon target bombarded with 20 MeV protons at the detection angle of 135°. The quasi-free electron bremsstrahlung and the secondary electron bremsstrahlung are the main components. Fig. 2 shows the comparison between the theoretical cross-sections of the bremsstrahlung with the experimentally derived cross-sections, which were measured previously [9]. The experimental error in the cross sections was within 17%.

The Compton tail background is the energy spectrum of the electrons recoiled by the Compton scattering of  $\gamma$ -rays inside the detector. This is estimated as follows:

$$N^{C.B.} = \frac{Q}{e} \times \frac{d\sigma_\gamma(\hbar\omega_\gamma)}{d\Omega} \cdot d\Omega \cdot n_M \cdot \delta x \cdot n_{Si} \delta x_{Si} \cdot \frac{d\sigma^{Compt}}{dE_e} \quad (6)$$

where  $d\sigma_\gamma(\hbar\omega_\gamma)/d\Omega$ ,  $d\sigma^{Compt}/dE_e$ ,  $\delta x$ ,  $n_{Si}$  and  $\delta x_{Si}$  are the production cross-sections of the  $\gamma$ -rays, the Compton scattering cross-section, the thickness of the target, the concentration of the Si semiconductor and the thickness of the X-ray detector, respectively.  $E_e$  is the energy of recoiled electron in the Compton scattering. In the case of  $E_e \ll m_e c^2$ ,  $d\sigma^{Compt}/dE_e$  is approximated to be constant, as follows [10]:

$$\frac{d\sigma^{Compt}}{dE_e} \approx \frac{2\pi r_0^2}{(\hbar\omega_\gamma)^2} m_e c^2 \quad (7)$$

We measured the production cross-sections of continuous X-rays from the carbon target bombarded with protons in the range 6 ~ 40 MeV and observed the Compton tails in the high energy region of the X-ray energy spectra [9]. We derived the component of the Compton tail from the X-ray spectrum as shown in Fig. 2. Fig. 3 shows the Compton tail as a function of proton energy with a Si(Li) detector thickness of 4.4 mm of which the experimental error was 17%.

Download English Version:

<https://daneshyari.com/en/article/8039342>

Download Persian Version:

<https://daneshyari.com/article/8039342>

[Daneshyari.com](https://daneshyari.com)